Natural-convection heat transfer in a nonuniform finite annulus with concentric heat source

Ming Lei and Clement Kleinstreuer
Department of Mechanical and Aerospace Engineering, North Carolina State University, Raleigh, NC, USA

In this paper, the mechanisms of natural-convection heat transfer inside a nonuniform finite annulus have been *numerically* investigated. The system is actually a streamlined, water-filled latex balloon with a coaxial cylindrical heating element. The balloon can be applied as a local hyperthermia treatment device for the removal of undesirable tissue if sufficiently high temperatures and preferably uniform surface heat fluxes can be maintained. A validated control-volume-based method has been employed to solve the coupled *transient three-dimensional* transport equations for laminar free convection. The effects of heat-source temperature distributions and device orientations on the heat transfer have been studied. Possible design improvements of this device are discussed.

Keywords: hyperthermia treatment device; transient three-dimensional free convection in nonuniform enclosure; numerical solution of velocity and temperature fields

Introduction

Laminar natural convection in vertical enclosures and horizontal annular spaces has been intensively investigated because of its basic importance in numerous engineering applications (Gebhart et al. 1988). For example, Kuehn and Goldstein (1976) measured temperature distributions for air and for water in a horizontal, long annulus with the inner cylinder heated. Ho et al. (1989) studied numerically free convection in concentric and eccentric horizontal cylindrical annuli with mixed boundary conditions. Kumar and Keyhani (1990) visualized the metastability of the flow structure in a horizontal cylindrical annulus with constant heat-flux condition for the inner surface and constant outer wall temperature. Ho and Lin (1991) extended their previous analyses to solve numerically and study experimentally the interactions of air/water convection in a horizontal annulus partially filled with cold water. All previous investigations of natural convection in annuli assumed steady two-dimensional (2-D) or axisymmetric flows. Numerical three-dimensional (3-D) free-convection studies focused primarily on flow instabilities in *rectangular* enclosures with different thermal boundary conditions, aspect ratios, and box orientations (cf. Yang 1988; Mukutmoni and Yang 1993; and others).

The present paper deals with transient 3-D buoyancy-driven flows in cylindrical enclosures of horizontal and vertical orientations. Specifically, the device can be used in local hyperthermia treatment (LHT) of undesirable tissue. It consists of a water-filled latex balloon that, inserted into a body cavity, takes on the shape of its surroundings. A concentric cylindrical heater with variable heat-shield temperature is the heat source (cf. Figure 1). The heat shield suppresses boiling and protects the balloon material from the heating element. The present application of the LHT device is for partial necrosis of the uterus lining in cases of menorrhagia (cf. Kleinstreuer and Lei 1994a). This is a safe and cost-effective procedure for the removal of tissue layers and hence a viable alternative to hysterectomies or other endometrial ablators employing lasers, microwaves, or electrodes as heat sources.

Analysis

Modeling equations

Considering transient 3-D incompressible flow with the Boussinesq approximation for the body force term and variable fluid Prandtl number, i.e., an iterative updating of the

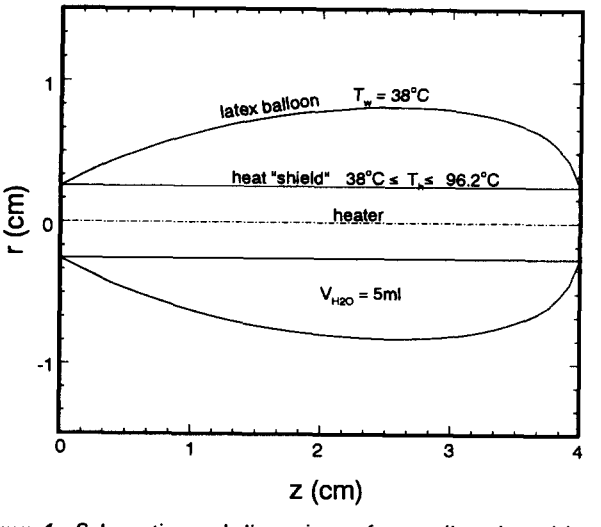

Figure 1 Schematics and dimensions of streamline-shaped latex balloon with concentric heater and heat shield

Address reprint requests to Professor Kleinstreuer at the Department of Mechanical and Aerospace Engineering, North Carolina State University, Box 7910, Raleigh, NC 27695-7910, USA.

Received 9 April 1994; accepted 20 July 1994

© 1994 Butterworth–Heinemann

temperature-dependent viscosity and thermal diffusion coefficients, the governing equations in dimensional form are (cf. Figure 1)

$$\text{(Continuity)} \quad \nabla \cdot \vec{v} = 0 \tag{1}$$

$$\text{(Momentum)} \quad \frac{\partial \vec{v}}{\partial t} + (\vec{v} \cdot \nabla)\vec{v} = -\frac{1}{\rho}\nabla p + \nabla \cdot (\nu \nabla \vec{v}) + \vec{g}\beta\Delta T \tag{2}$$

$$\text{(Energy)} \quad \frac{\partial T}{\partial t} + (\vec{v} \cdot \nabla)T = \nabla \cdot (\alpha \nabla T) \tag{3}$$

where the velocity vector is $\vec{v} = (v_r, v_\theta, v_z)$ and the volumetric expansion coefficient is $\beta = -1/\rho(\partial\rho/\partial T)_p$. The momentum equation (Equation 2), for which $\Delta T = T - T_0$, depends on the thermal energy equation (Equation 3), which in turn requires the velocity field for solution. Typical system parameter values for water at $T_0 = 38°C$ are listed in Table 1.

Initially, the preheated water is at $T_0 = 38°C$ and the concentric heat source temperature is $T_h(t = 0) = 38°C$. Then the cylindrical wall temperature increases with time to $T_{h,\max}(t \geq 80 \text{ sec}) = 96.2°C$ (cf. Figure 2a) with either a uniform or a trapezoidal *axial* distribution, as given in Figure 2b. These surface-temperature characteristics are measured design values from actual electrical resistance heaters (cf. Kleinstreuer and Lei 1994a). The isothermal balloon surface is kept at body temperature, i.e., $T_w = 38°C$, which is a reasonable assumption in light of the strong perfusion of organ tissues.

Solution method

The transport equations (Equations 2 and 3), subject to the mass conservation law (Equation 1) and the initial/boundary conditions outlined, can be rewritten in compact form for the control volume solution method (cf. Patankar 1980). In general,

$$\frac{\partial}{\partial t}(\rho\phi) + \text{div}(\rho\vec{v}\phi) = \text{div}(\Gamma_\phi \nabla\phi) + S_\phi \tag{4}$$

Table 1 System parameters for water at 38°C

Balloon length (axial)	$L = 4$ cm
Maximum radius (streamline shape)	$r_{max} = 8.2$ mm
Balloon volume	$\forall \geq 5$ ml
Initial or reference temperature	$T_o = 38°C$
Prandtl number	$Pr = 4.608$
Aspect ratio, L/r_{max} (vertical orientation)	$A \approx 7$
Volumetric expansion coefficient	$\beta = 1.8 \times 10^{-4}\ K^{-1}$
Grashof numbers (horizontal)	$Gr_r = 3.874 \times 10^4$,
(vertical)	$Gr_L = 2.73 \times 10^5$
Rayleigh number	$Ra_L = Gr_L\,Pr = 1.26 \times 10^6$
Reference velocity (steady-state)	$u_{ref} = 1.123 \times 10^{-2}$ m/s
Reynolds number, $u_{ref}\, r_{max}/\nu$	$Re_r = 92$

where the four terms represent the local time-rate-of-change of ϕ, the net convection, net diffusion, and all sinks and sources affecting ϕ. The dependent variable ϕ is equivalent to the velocity components v_r, v_θ, and v_z, as well as the temperature T. The generalized diffusion coefficient, Γ_ϕ, could be the viscosity μ when ϕ represents a velocity component and k/c_p when ϕ is the temperature. Whatever cannot be accommodated with the first three terms can always be expressed as (a part of) the source term. For example, the pressure gradient and the buoyancy force term in the momentum equations, or the heat fluxes across boundaries, are represented as source terms.

Employing a nonlinear operator $L(\cdot)$, Equation 4 can be rewritten in normal form as

$$L(\phi) = 0 \tag{5a}$$

or with an unknown approximate solution $\bar{\phi}$,

$$L(\bar{\phi}) = R \tag{5b}$$

where R is the residual of $L(\bar{\phi})$. Now, the weighted residual is forced to be zero over the entire computational domain. Specifically, the flow field is divided into nonoverlapping control volumes $V_i (i = 1, 2, \ldots, N)$, and the weighting function

Notation

A	Aspect ratio, $L/\Delta r_{max}$
a_p, a_E, etc.	Coefficients in the CVM formulation
c_p	Specific heat (J/kg·°C)
g	Gravity (m/s²)
Gr	Grashof number, $g\beta\Delta T\Delta r_{max}^3/\nu^2$
k	Thermal conductivity (W/m°C)
L	Axial device length (m)
L_s	Balloon surface length (m)
p	Pressure (N/m²)
Pr	Prandtl number, ν/α
q_w	Surface heat flux (J/m²·s)
Δr_{max}	Maximum distance of the annulus gap (m)
Ra	Rayleigh number, Gr·Pr
Re	Reynolds number, $u_{ref}\Delta r_{max}/\nu$
s	Coordinate along balloon surface (m)
S, b	Source term in the CVM formulation
t	Time (s)
T	Temperature (°C)
T_o	Initial or reference temperature (°C)
T_c	Critical temperature (°C)
u_{ref}	Reference velocity, $(g\beta\Delta T_{max}\Delta r_{max}/Pr)^{1/2}$(m/s)
$\vec{v}$	Velocity vector (m/s)
v_r, v_θ, v_z	Velocity components in the r, θ, z directions, respectively (m/s)
z	Axial coordinate (m)

Greek symbols

α	Thermal diffusivity, $k/\rho c_p$ (m²/s)
β	Thermal expansion coefficient $-\frac{1}{\rho}\left(\frac{\partial\rho}{\partial T}\right)_p$ (K⁻¹)
Γ	Diffusivity in the CVM formulation
ν	Kinematic viscosity (m²/s)
ρ	Reference density of the fluid (kg/m³)
ϕ	Dependent variable in the CVM formulation
∇	Gradient operator (1/m)

Subscripts

h	Heat shield
L	Parameter values based on length scale L
r	Parameter values based on length scale r_{max}
max	Maximum value
o	Initial
w	Wall value
ϕ	Related to dependent variable ϕ

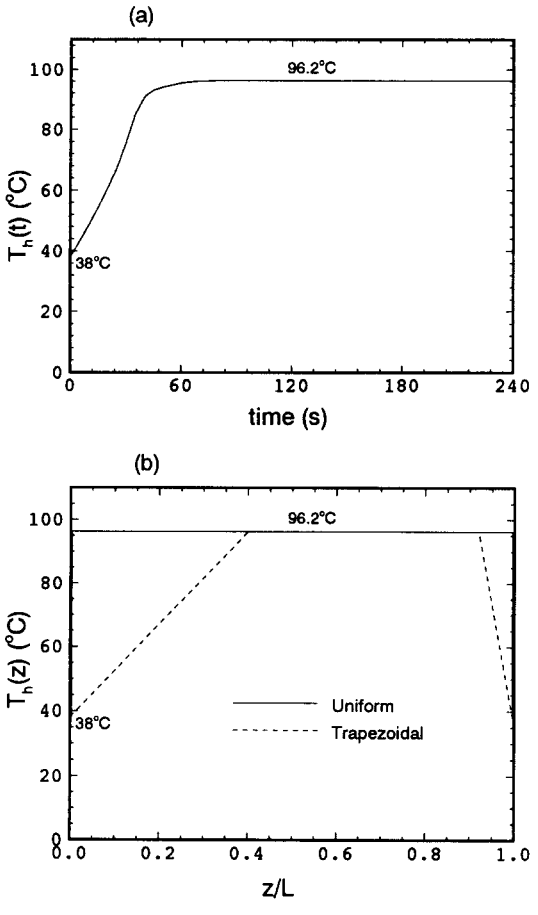

Figure 2 (a) Temporal and (b) spatial heat-shield temperature distributions

is set to be unity over one subdomain at a time and zero elsewhere:

$$\int_{V_i} R_i d\forall = 0; \qquad i = 1, 2, \ldots, N \tag{6}$$

As a result, N algebraic weighted-residual equations are obtained to calculate the value of $\bar{\phi}$ for each control volume, assuring conservation of mass, momentum, and thermal energy. Specifically,

$$a_p\phi_p = a_E\phi_E + a_W\phi_W + a_N\phi_N + a_S\phi_S + a_H\phi_H + a_L\phi_L + b \tag{7}$$

where ϕ_p, ϕ_E, etc., are the unknown values of the dependent variable ϕ at the nodal point p and its neighboring nodal points in the directions E, W, N, S, H, and L for 3-D flows; a_p, a_E, etc., are coefficients that depend on the type of finite-difference approximation employed, e.g., upwind differencing for the convective terms, to evaluate gradients at the control surfaces.

The variable-density control-volume meshes for one half of a nonuniform finite annulus and its cross-sectional area at $z/L = 0.51$ are shown in Figures 3a and 3b. A total of 19,552 elements were necessary. Trial and error runs with further mesh refinements did not change the results, which indicates that mesh independence had been achieved. Variable time steps, i.e., $5 \text{ sec} \leq \Delta t \leq 20 \text{ sec}$, were employed to accurately simulate the transient, $0 < t \leq 50$ sec, intermediate, $50 \leq t \leq 100$ sec, and steady-state phases. About 30 iterations were needed for convergence during the transient phase and two to four sweeps for $t > 70$ sec.

The numerical calculations have been carried out on an IBM RISC/6000 workstation. Typical CPU times ranged from five minutes for the vertical axisymmetric case to five hours for the horizontal 3-D case. The convergence criterion of mass residual was less than 1.0×10^{-6}.

Results and discussion

Of interest are the temperature distributions and balloon-surface heat fluxes for the innovative LHT device in horizontal and vertical orientations. Some related velocity fields are discussed by Kleinstreuer and Lei (1994b).

There are two critical heat transfer parameters that have to be achieved for the device to work effectively. A minimum (water) temperature of 45°C is necessary to kill cells within a circumscribed area, while a quasi-uniform wall heat flux has to be sustained so that the excessive heat can penetrate into the tissue, typically 4 to 5 mm deep. As in the present device application, it is often desirable to treat hyperthermally only a portion, say 30 to 70 percent, of the diseased area. Before the convection heat transfer results are discussed, the validation of the computer simulation model is briefly documented.

Model validation

There are two system comparisons that indicate that the present computer simulation model is accurate. The first system is that of a heated horizontal cylinder in a fluid reservoir where the steady-state isotherms near the cylinder (cf. Gebhart et al. 1988) are the same as the temperature contours shown in Figure 7a below for the midsection of the LHT device in horizontal position. The second system consisted of a small water-filled beaker (i.e., $\forall = 30$ ml) with a concentric cylindrical heater element. A thermocouple located off-center at $r/r_o = 0.588$ was used to measure $T(t)$ while the device was in a constant-temperature bath of $T_w = 38$°C. Figure 4 shows the comparison between a computed point temperature with time and measurements (cf. WATLOW 1991). The agreement between the predicted results and the experimental observations is excellent.

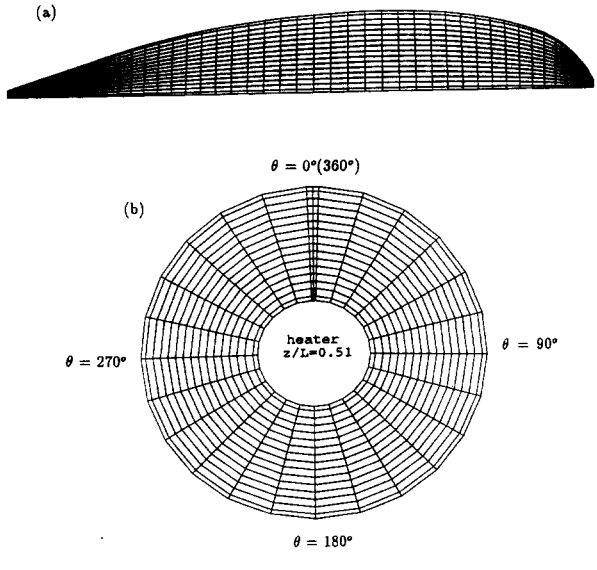

Figure 3 Control volume mesh for water-filled balloon. (a) Midplane of upper half; (b) cross section at $z/L = 0.51$

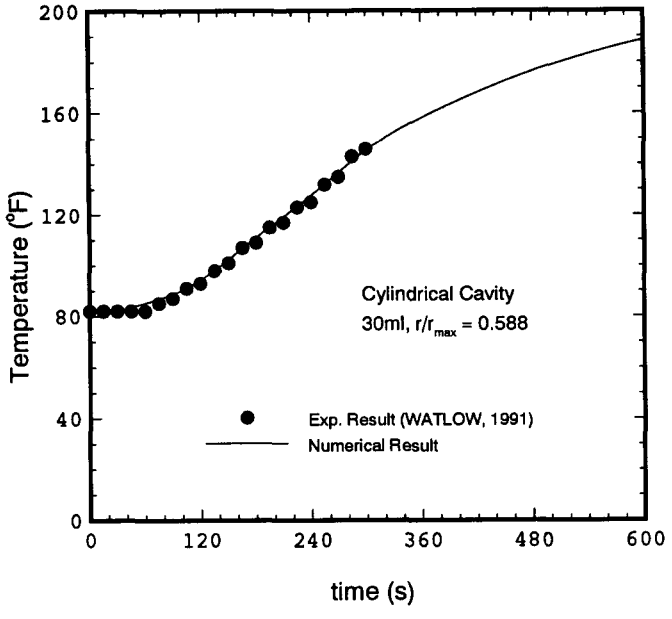

Figure 4 Experimental data comparison for transient point temperature in a cylindrical cavity

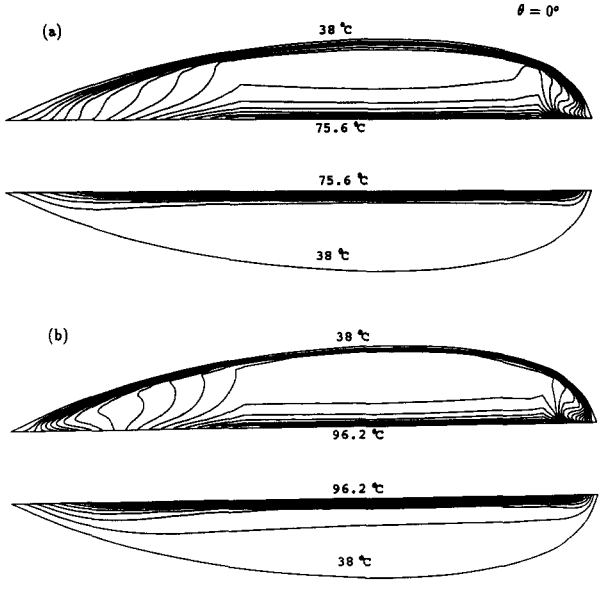

Figure 5 Vertical midplane isotherms of balloon water due to trapezoidal heat-shield temperature profile at (a) transient state ($t = 30$ sec) and (b) steady state ($t = 240$ sec)

Horizontal device-orientation

The transient thermal boundary condition $T_h(t, z)$ along the concentric heater surface generates 3-D temperature fields as depicted in Figures 5 to 8. Isotherms in the *vertical midplane* are shown in the time-dependent phase at $t = 30$ sec (cf. Figure 5a) and at steady state (cf. Figure 5b). At $t = 30$ sec, the heat-shield temperature with a trapezoidal axial distribution has reached $T_h = 75.6°C$; heat is convected upwards in the main part of the upper balloon half ($u_{ref} \approx 0.8 \times 10^{-2}$ m/sec) and convected sidewards towards the head and tail portions of the device. The resulting temperature field in the upper half is entirely free-convection dominated. Although all rising fluid is coming down along the balloon wall, the heat-convection effect is hardly noticeable in the lower half of the balloon. There, the heat transfer is due to conduction near the heat shield, and at the bottom most of the water stays at $T_w = 38°C$ (Figure 5a). Steady state is reached after $t \approx 80$ sec, when the maximum heater surface or heat-shield temperature $T_{h,max} = 96.2°C$. Buoyancy-induced flow in the upper half has increased measurably, with $u_{ref} = 1.123 \times 10^{-2}$ m/sec. This influences the lower half somewhat; however, a large portion remains at $T_w = 38°C$ (cf. Figure 5b). For the *horizontal midplane*, symmetry permits grouping the isotherms at two different time levels into one graph. Thus, Figure 6 depicts narrowing temperature contours and hence a rapid increase in wall heat flux with time.

Steady-state isotherms at three different cross sections, namely, $z/L = 0.510$ (center), $z/L = 0.111$ (tail end), and $z/L = 0.944$ (head), are shown in Figures 7a to 7c. The contours at $z/L = 0.51$ are very similar to the isotherms in *infinite* cylindrical annuli, whereas significant differences appear in the

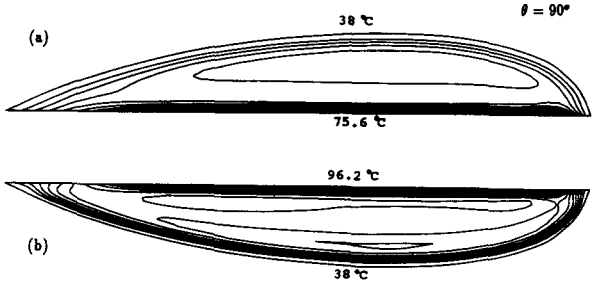

Figure 6 Horizontal midplane isotherms due to trapezoidal heat-shield temperature profile at (a) $t = 30$ sec and (b) $t = 240$ sec

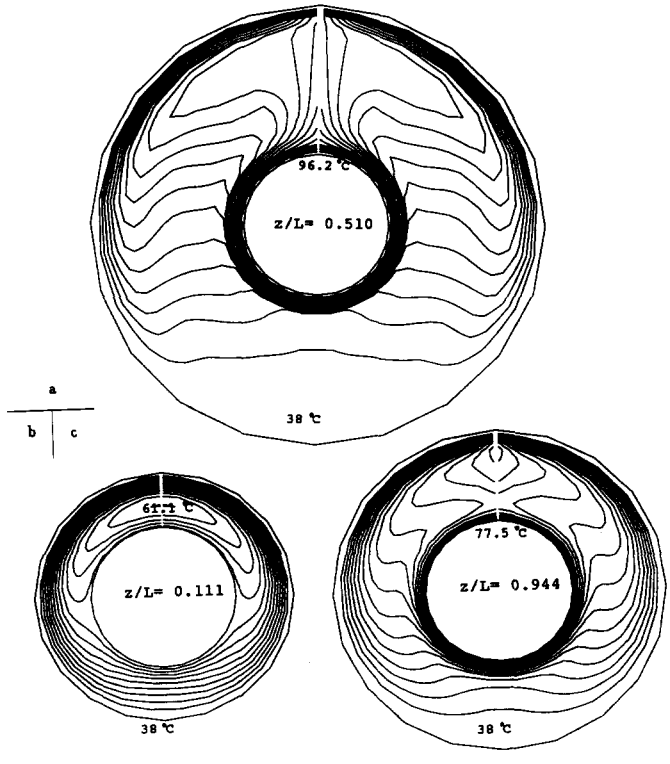

Figure 7 Steady-state isotherms in three cross sections due to trapezoidal heat-shield temperature profile at (a) $z/L = 0.510$ (center), (b) $z/L = 0.111$ (tail end), and (c) $z/L = 0.944$ (head)

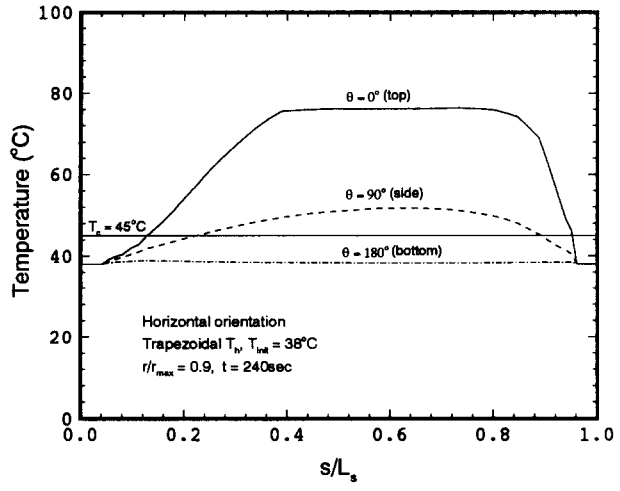

Figure 8 Steady-state temperature profiles at three circumferential locations in *near-wall* axial direction

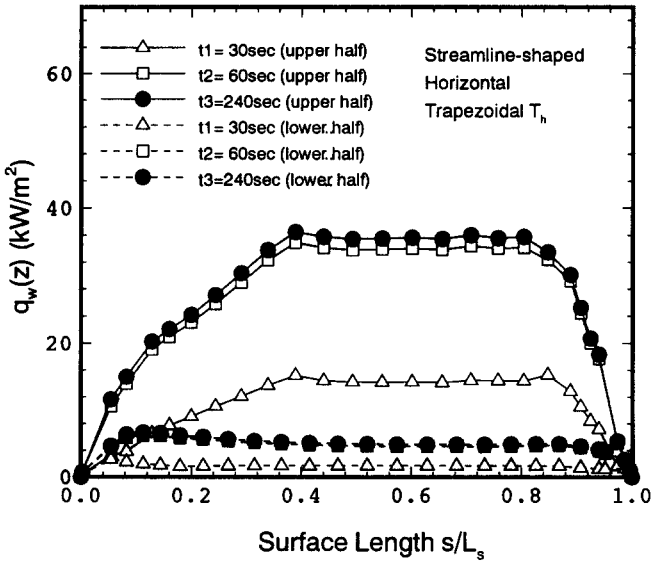

Figure 9 Area-averaged balloon surface heat-flux distribution for upper half and lower half at different time levels due to trapezoidal heat-shield temperature profile

front part of the balloon and especially in the tail end because of 3-D effects.

The previous graphs can be summarized in terms of (steady-state) temperature profiles in the axial direction along the balloon surface at $r/r_{max} = 0.9$ (cf. Figure 8) for different circumferential locations, i.e., $\theta = 0°$ (top), $\theta = 90°$ (side), and $\theta = 180°$ (bottom). As expected, the near-top temperature is highest, with a rather uniform distribution. Almost the entire upper half of the device exceeds the critical temperature, $T_c = 45°C$, for necrosis. The resulting balloon-surface heat fluxes with time, averaged for the upper and lower halves, are given in Figure 9. The maximum $\bar{q}_w$ for the upper part of the device is about eight times larger than for the lower portion. If a uniform heat-shield temperature is chosen, then $\bar{q}_w$ is more uniform over the entire balloon surface (cf. Figure 10).

Vertical device-orientation

The device in the vertical position reduces to an axisymmetric problem. The steady-state velocity field and constant temperature contours are shown in Figure 11. With the relatively high Rayleigh number $Ra = O(10^6)$ (cf. Table 1), unicellular boundary-layer-type flow is quickly established. The elongated core of the half-domain is nearly stagnant, which results in conduction-dominated heat transfer, as seen by the linear segments of the isotherms. With the warmer water accumulating in the top section and then coming down the cooler balloon surface, the axisymmetric wall heat flux exhibits a sharp maximum near the top (cf. Figure 12). Hence, in this configuration, only a limited ringlike portion of the device can be effectively used.

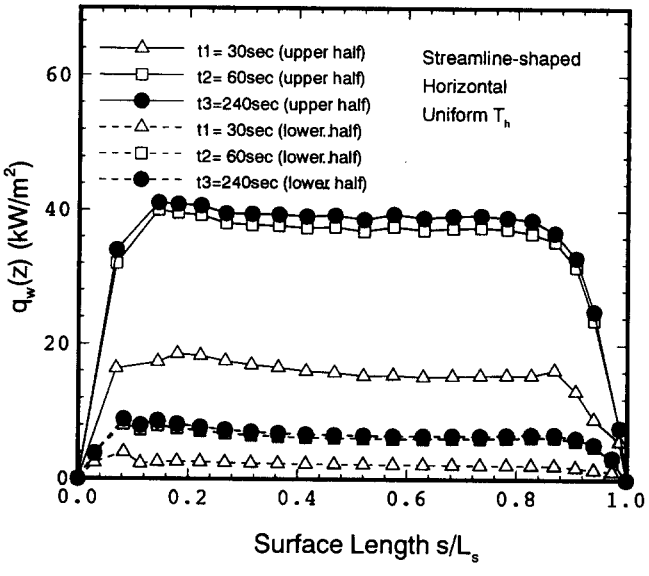

Figure 10 Area-averaged balloon-surface heat-flux distribution for upper half and lower half at different time levels due to uniform heat-shield temperature profile

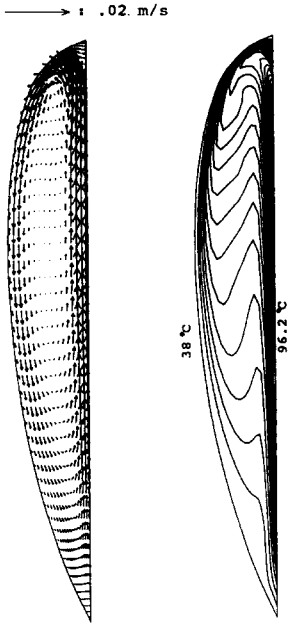

Figure 11 Steady-state velocity vector plot and isotherms for water-filled balloon in vertical position with trapezoidal heat-shield temperature profile

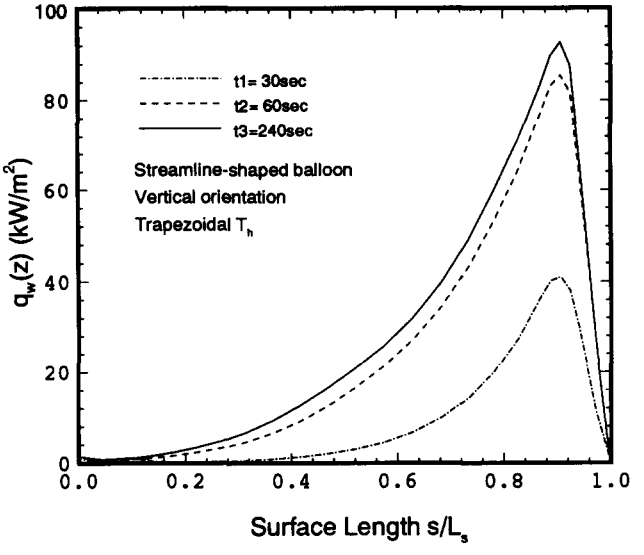

Figure 12 Local surface heat-flux profiles at three time levels for vertical device orientation

Device improvements

For the device in the *vertical* position, insertion of horizontal disklike latex walls, which generate discrete compartments, will break up the unicellular flow field and should produce a more uniform near-wall temperature distribution and surface heat flux. For the device in the *horizontal* position, higher heater surface temperatures will cause boiling and hence more rigorous mixing, which should destroy the stably stratified lower balloon region. However, this result would present a formidable two-phase flow problem, where the pressure buildup due to steam formation would have to be monitored.

Changes in initial temperature, e.g., $T_0 = 20°C$, and balloon shape, i.e., pear-shaped vs. streamline-shaped, had only secondary effects on the surface heat-flux distributions as discussed in Kleinstreuer and Lei (1994a, 1994b).

Conclusions

The problem of transient 3-D free convection in an arbitrary enclosure has been solved numerically using the control-volume method. The validated computer simulation model has been applied to the analysis and design of a water-filled latex balloon that can be used in the local hyperthermia treatment (LHT) of undesirable tissue. Of interest are the liquid-side temperature profiles near the balloon surface and the wall heat-flux distributions for different heat-source boundary conditions and device orientations. The results of the computational heat transfer studies can be summarized as follows:

- the thermal wall condition of the concentric heating element and the balloon orientation are the most important design parameters of the LHT-device;
- the device in the *horizontal* orientation is in the upper half free-convection dominated and the lower half heat-conduction controlled. Three-dimensional effects are especially significant in the front and tail end of the nonuniform, finite annulus. As a result of the buoyancy-driven heat transfer, more than half of the balloon surface can be effectively used for undesirable tissue ablation;
- the device in the *vertical* position reduces to an axisymmetric free-convection problem with an effective balloon surface area of less than 30%; and
- the performance improvement of the LHT device that should be considered is better fluid mixing in the *lower* balloon regions. This result could be achieved with higher heater surface temperatures causing multicellular flow patterns (e.g., $Ra \geq 10^6$), turbulence, and/or boiling. Other future work should include the coupled bioheat equation for the surrounding multilayer tissues in order to *compute* the transient interfacial temperature rather than assuming a constant surface temperature.

References

Gebhart, B., Jaluria, Y., Mahajan, R. L., and Sammakia, B. 1988. *Buoyancy-Induced Flows and Transport*. Hemisphere, New York

Ho, C. J., Lin, Y. H., and Chen, T. C. 1989. A numerical study of natural convection in concentric and eccentric horizontal cylindrical annuli with mixed boundary conditions. *Int. J. Heat Fluid Flow*, **10** (1), 40–47

Ho, C. J. and Lin, Y. H. 1991. Natural convection in a horizontal annulus partially filled with cold water. *Int. J. Heat Mass Transfer*, **34** (6), 1371–1382

Kleinstreuer, C. and Lei, M. 1994a. A new Local Hyperthermia Treatment device for partial tissue necrosis. *ASME J. Biomech. Eng.* (in press)

Kleinstreuer, C. and Lei, M. 1994b. Transient laminar three-dimensional fluid flow fields in slender enclosures with coaxial heated cylinder. *Int. J. Eng. Sci.*, **32** (10), 1635–1646

Kuehn, T. H. and Goldstein, R. J. 1976. An experimental and theoretical study of natural convection in the annulus between horizontal concentric cylinders. *J. Fluid Mech.*, **74**, 695–719

Kumar, R. and Keyhani, M. 1990. Flow visualization studies of natural convective flow in a horizontal cylindrical annulus. *ASME J. Heat Transfer*, **112**, 784–787

Mukutmoni, Q. and Yang, K. T. 1993. Rayleigh–Benard convection in a small aspect ratio enclosure, Part I and Part II. *ASME J. Heat Transfer*, **115**, 360–376

Patankar, S. V. 1980. *Numerical Heat Transfer and Fluid Flow*. Hemisphere, Washington, DC

WATLOW, 1991. Experimental data sets for cartridge heater and beaker temperature study. Consulting Report for Ed. WECK, Research Triangle Park, NC

Yang, K. T. 1988. Transitions and bifurcations in laminar buoyant flows in confined enclosures. *ASME J. Heat Transfer*, **100**, 1191–1204